Carbohydrate Polymers 91 (2013) 7–13

Contents lists available at SciVerse ScienceDirect

Carbohydrate Polymers

journal homepage: www.elsevier.com/locate/carbpol

Fabrication and properties of chitin/hydroxyapatite hybrid hydrogels as scaffold nano-materials

Chunyu Chang[a,b,c], Na Peng[b,c], Meng He[a], Yoshikuni Teramoto[c], Yoshiyuki Nishio[c], Lina Zhang[a,*]

[a] Department of Chemistry, Wuhan University, Wuhan 430072, China
[b] Guangzhou Sugarcane Industry Research Institute, Guangzhou 510316, China
[c] Division of Forest and Biomaterials Science, Graduate School of Agriculture, Kyoto University, Sakyo-ku, Kyoto 606-8502, Japan

ARTICLE INFO

Article history:
Received 28 May 2012
Received in revised form 17 July 2012
Accepted 27 July 2012
Available online 3 August 2012

Keywords:
Chitin
Nano-hydroxyapatite
Hybrid hydrogel
Scaffolds

ABSTRACT

Novel hybrid hydrogels were prepared by introducing nano-hydroxyapatite (nHAp) into chitin solution dissolved in NaOH/urea aqueous solution at low temperature, and then by cross-linking with epichlorohydrin (ECH). Their structure and morphology were characterized by FTIR spectra, wide-angle X-ray diffraction (WAXD), thermo-gravimetric analysis (TGA), scanning electron microscopy (SEM), and transmission electron microscopy (TEM). Our findings revealed that hydroxyapatite nano-particles were uniformly dispersed in chitin hydrogel networks. The chitin/nHAP hybrid hydrogel (Gel2) exhibited about 10 times higher mechanical properties (compressive strength: 274 kPa) than that of chitin hydrogel. Moreover, COS-7 cell culture experiment proved that cells could adhere and proliferate well on the chitin/nHAp hydrogels, suggesting good biocompatibility. All these results signified that these biomaterials could be potential candidates as scaffolds for tissue engineering.

1. Introduction

Hydrogels are water-swollen polymeric materials that maintain distinct three-dimensional networks, with the ability to absorb and retain a significant amount of water. Since the discovery of hydrogels as contact lenses (Zohuriaan-Mehr, Omidian, Doroudiani, & Kabiri, 2010), the hydrogel applications are now widespread in the fields of agriculture (Kopecek, 2009), drug delivery (Hoare & Kohane, 2008), sensors (Richter et al., 2008), and so on. Especially, biodegradable hydrogels are currently used as scaffolds in tissue engineering, where the 3D networks may contain cells to repair defective tissue, due to hydrogels having structural similarity to the macromolecular-based components in the body and are considered biocompatible (Lee & Mooney, 2001). There are two major types of hydrogels, synthetic and natural hydrogels, according to their origin. Synthetic hydrogels are made mainly from synthetic polymers, such as poly(acrylic acid), poly(ethylene glycol), poly(vinyl alcohol), polyacrylamide, and polypeptide (Ryan & Nilsson, 2011; Zhu, 2010). Natural hydrogels are from biopolymer-based materials, such as polysaccharides (including hyaluronic acid, chitosan, alginate, and cellulose) and proteins (e.g., elastin, collagen, gelatin, fibrin, and globular proteins) (Jonker, Lowik, & van Hest, 2012; Van Vlierberghe, Dubruel, & Schacht, 2011).

Hydroxyapatite (HAp) exhibits excellent biocompatibility with soft tissue such as skin, muscle and gums, so it has become an ideal candidate for orthopedic and dental implants or components of implants (Zhou & Lee, 2011). However, the intrinsic properties of HAp, such as hardness, fragility, and lack of flexibility, make it difficult to be shaped in the specific form required for bone repair and implantation, which limits its application as a load-bearing implant scaffold material (Sun, Zhou, & Lee, 2011). Therefore, many studies have been reported on composite materials containing HAp in combination with various polymers, such as poly(lactic acid), sodium alginate, cellulose, polycaprolactone, collagen, and chitosan, to overcome the drawbacks of HAp for the application in tissue engineering (Cai et al., 2011; Eosoly, Brabazon, Lohfeld, & Looney, 2010; Grande, Torres, Gomez, & Carmen Bañó, 2009; Jeong et al., 2008; Rossi et al., 2012; Swetha et al., 2010; Tan et al., 2010; Zhang et al., 2010). These polymers have been widely used to develop porous 3D scaffolds. Usually, natural polymer-based composites have been focused with more attention than synthetic polymer composite for bone tissue engineering applications, due to the biocompatible and biodegradable behavior of natural polymers. Chitin is produced by a number of living organisms in lower plant and animal kingdoms, and possesses natural biocompatibility, which is very good candidate of biomaterials. It is noted that nano-sized HAp (nHAp) which has high surface area to volume ratio showed significant improved properties such as bioactivity

* Corresponding author. Tel.: +86 27 87219274; fax: +86 27 68754067.
E-mail addresses: lnzhang@public.wh.hb.cn, linazhangwhu@gmail.com (L. Zhang).

0144-8617/$ – see front matter © 2012 Elsevier Ltd. All rights reserved.
http://dx.doi.org/10.1016/j.carbpol.2012.07.070

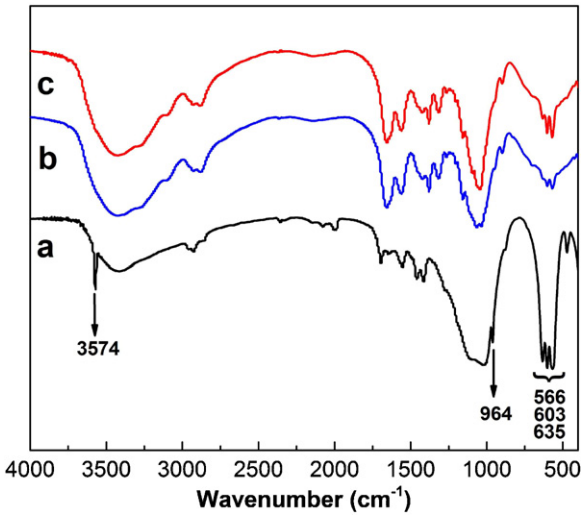

Fig. 1. FTIR spectra of nano-hydroxyapatite (a), Gel1 (b), and Gel2 (c).

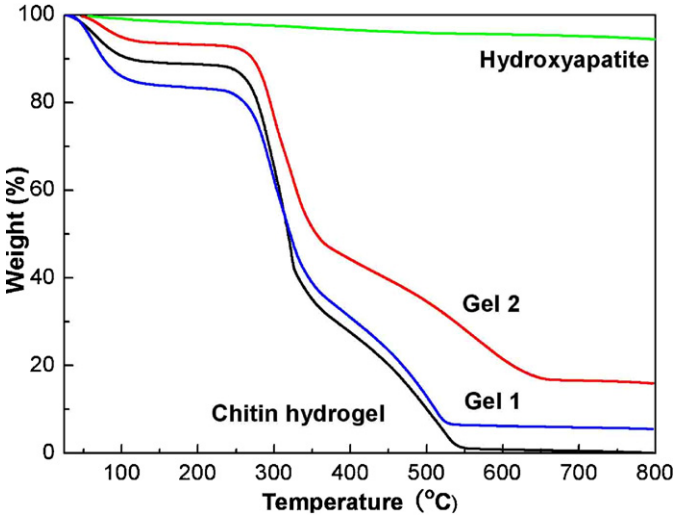

Fig. 2. TGA curves of nano-hydroxyapatite, chitin hydrogel, Gel1, and Gel2.

including osteoblast adhesion, osteoconductivity, and osseointegration, protein adsorption, and mechanical strength (Kumar et al., 2011; Wei & Ma, 2004). Therefore, the inclusion of nHAp into polymer matrix can not only improve the mechanical properties but also incorporate the nanotopographic features that mimic the nanostructure of natural bone.

In our previous work, chitin hydrogels were fabricated by dissolving chitin in NaOH/urea aqueous solution at low temperature. These hydrogels were non-toxic and had good biocompatibility (Chang, Chen, & Zhang, 2011). However, they are not bioactive to induce desired bone regeneration. Herein, we attempted to construct chitin/nHAp hydrogels as scaffolds for tissue engineering, where chitin hydrogels were used as matrix for nHAp. The structure and morphology of the hydrogels were characterized by wide-angle X-ray diffraction (WAXD) and scanning electron microscopy (SEM). The content and distribution of nHAp in chitin hydrogels were determined by thermo-gravimetric analysis (TGA) and transmission electron microscopy (TEM). Moreover, the mechanical properties and biocompatibility of hydrogels were also evaluated.

2. Experimental

2.1. Materials

Chitin powder was purchased from Jinke Chitin Co. Ltd. (Zhejiang, China). The degree of acetylation (DA) was determined by elemental analysis to be 0.98. The weight-average molecular weight (M_w) and radius of gyration ($\langle S^2 \rangle^{1/2}$) of chitin, measured by dynamic light scattering (DLS, ALV/CGS-8F, ALV, Germany) in 5% LiCl/DMAc (w/w), were 5.0×10^5 and 68 nm, respectively. $Ca(NO_3)_2{\cdot}4H_2O$, $(NH_4)_2HPO_4$ (Sinopharm Chemical Reagent Co. Ltd.), NaOH, $NH_3{\cdot}H_2O$, and urea (Shanghai Chemical Reagent Co. Ltd., China) were used as received. Epichlorohydrin (ECH, Chemical Agents, Ltd. Co., Shanghai, China) (density, 1.18 g/mL) was analytical-grade and used without further purification. COS-7 cells were obtained from China Typical Culture Center (Wuhan University) and cultured in Dulbecco's modified Eagle's medium (DMEM, Sigma) supplemented with 4 mM L-glutamine, 10% fetal bovine serum (FBS), antibiotics (100 U/mL penicillin and 100 μg/mL streptomycin) at 37 °C in a humidified air atmosphere containing 5% CO_2.

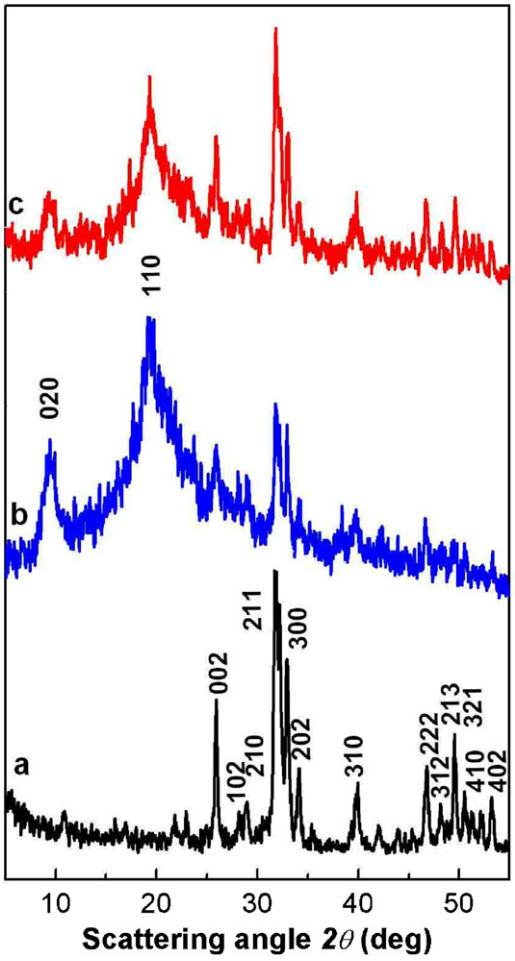

Fig. 3. WAXD patterns of hydroxyapatite (a), Gel1 (b), and Gel2 (c).

2.2. Preparation of chitin/nano-hydroxyapatite hydrogels

Nano-hydroxyapatite (nHAp) was prepared according to our previous work as follows (He, Chang, Peng, & Zhang, 2012). $Ca(NO_3)_2$ solution was added into $(NH_4)_2HPO_4$ solution with stirring, and the pH of solution was adjusted by $NH_3{\cdot}H_2O$ to be 10. The mixture was stirred for 2 h and the nHAp precursor was

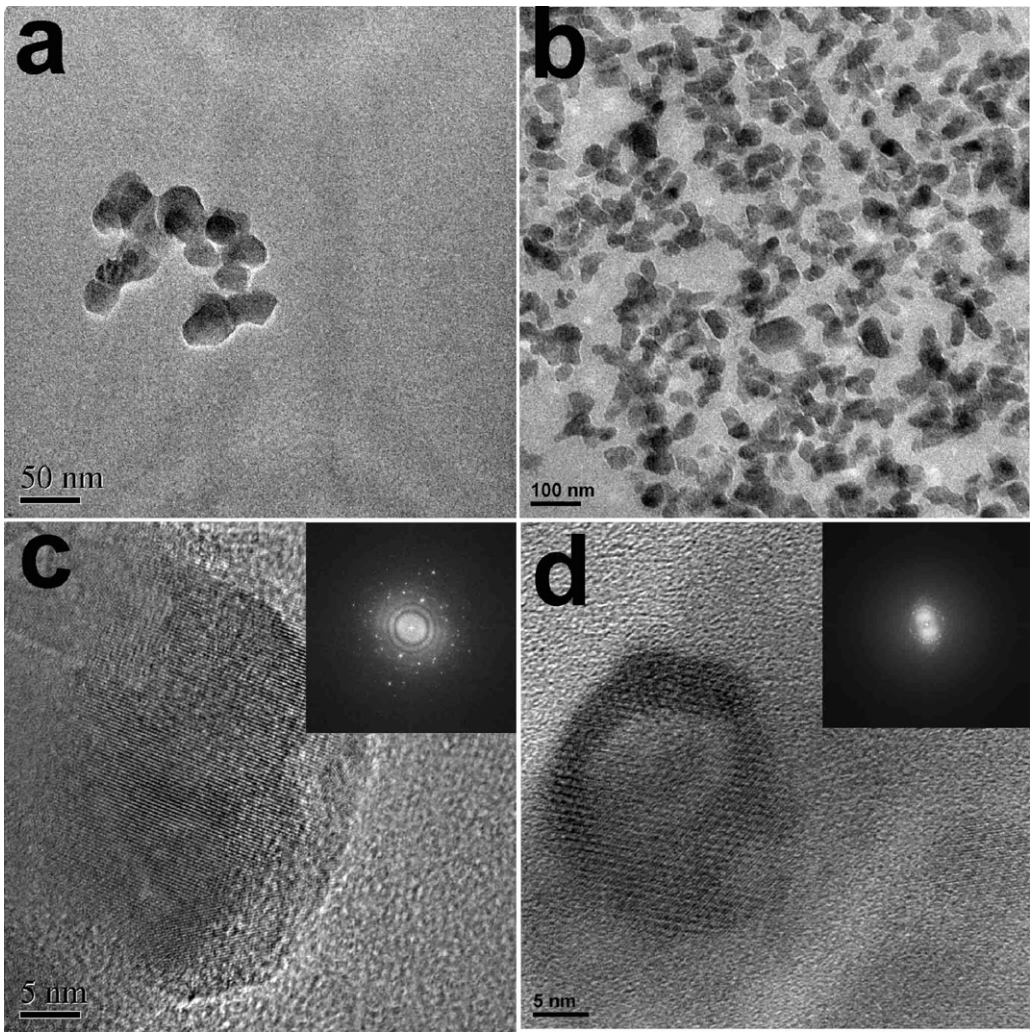

Fig. 4. TEM images of hydroxyapatite particles in butyl alcohol (a and c) and Gel2 (b and d).

aged for 12 h at 25 °C, filtered, and rinsed with absolute ethanol. The obtained product was ground by a pestle before calcination at 600 °C to get nanoparticles. Desired amounts of the HAp nanoparticles were dispersed in chitin solvent (8 wt% NaOH/4 wt% urea/88 wt% water) and treated in ultrasonic bath for 30 min with a KQ3200 ultrasonic instrument (Kunshan Ultrasonic Instrument Co., Ltd., Kunshan, China). Then, a chitin solution was obtained by dissolving 0.2 g chitin in 10 g solvent through freezing/thawing (−20 °C/room temperature) method (Chang et al., 2011). 1 mL ECH as cross-linking agent was added into 10 g solution under stirring for 30 min. After reacting at 60 °C for 1 h, chitin/nHAp hydrogels were taken out carefully and washed with distilled water to remove alkali, urea, and excess ECH. The weight ratio (chitin/nHAp) of samples was 8/1 and 4/1, coded as Gel1 and Gel2, respectively.

2.3. Characterization

The vacuum dried samples were analyzed in KBr discs by FTIR (Perkin Elmer Spectrum One, Wellesley, MA, USA) in the region of 400–4000 cm^{-1}. Thermo-gravimetric analysis (TGA) of the dry samples (5 mg) was carried out on a Pyris TGA linked to a Pyris diamond TA Lab System (Perkin-Elmer Co., USA) at a heating rate of 10 °C min^{-1} from 40 to 800 °C under N_2 atmosphere. The wide-angle X-ray diffraction (WAXD) pattern of the dried sheets was recorded on a WAXD instrument (XRD-6000, Shimadzu, Japan) with Cu K_α radiation ($\lambda = 0.154$ nm). WXRD data were collected from $2\theta = 4$–40° at a scanning rate 1°/min.

Scanning electron micrograph (SEM) measurements were carried out on a Hitachi X-650 microscope (Japan). The hydrogels swollen to equilibrium in distilled water at 25 °C for 24 h were frozen in liquid nitrogen and snapped immediately, and then freeze-dried. The fracture surface (cross-section) of the hydrogel was sputtered with gold, and was observed and photographed. TEM observation of the HAp nanoparticles in butyl alcohol and chitin/nHAp hydrogel was carried out on a JEM-2010 FEF (UHR) transmission electron microscope (JEOL TEM, Japan). Samples were prepared by evaporating a drop of suspension on a carbon coated copper grid (for butyl alcohol) and slicing for ultrathin section (for chitin/nHAp hydrogel).Dynamic mechanical analysis (DMA, TA instrument Q800 series) was used to determine the compressive modulus of the swollen hydrogel samples. To reach swelling equilibrium, hydrogels were incubated in distilled water for 24 h at room temperature before the test. The disk shaped samples were 1 cm × 0.5 cm (diameter × height) in dimension and were tested in compression mode at 25 °C. Young's modulus of samples was calculated by the ratio of stress and strain at break point.

2.4. Cell viability assay

Chitin/nHAp hydrogels were sterilized with ethanol (70%) and followed by air drying. COS-7 cells were seeded on the surface of

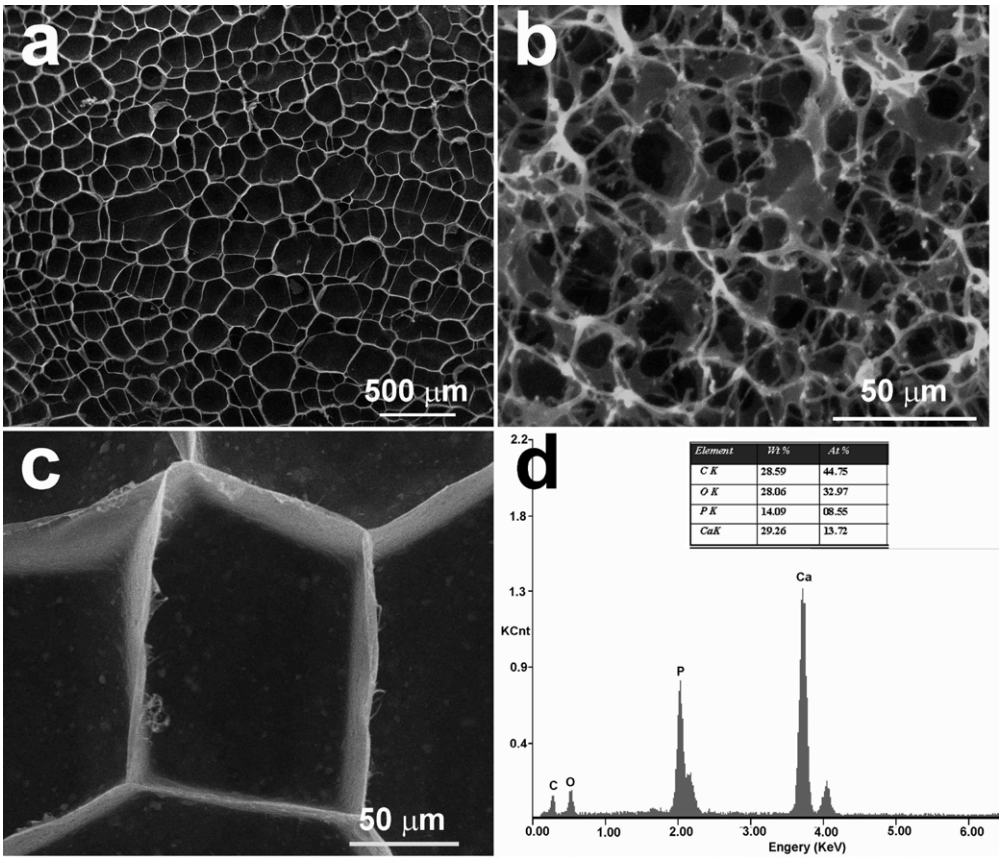

Fig. 5. SEM images of chitin/HAp hydrogel (Gel2): surface (a and c), cross-section (b), and energy-dispersive spectrum (EDS) from SEM (d).

hydrogels (80,000 cells/well) in 24-well plates in DMEM with 10% FBS, and incubated at 37 °C under 5% CO_2 for 24 h. Then, cells were rinsed twice with phosphate buffer solution (PBS). 200-μL PBS containing calcein-AM (2 μM) and ethidium homodimer-1 (4 μM) was added to each well for staining cells at 37 °C under 5% CO_2 for 30 min. The stained cells were observed by a confocal laser scanning microscope (Nikon, TE2000, EZ-C1, Japan).

3. Results and discussion

3.1. Structure and miscibility of chitin/nHAp hydrogels

FTIR spectra of hydroxyapatite nanoparticles and chitin/nHAp hydrogels are shown in Fig. 1. The absorption band at 3574 cm^{-1} was corresponding to stretching vibration of hydroxyl groups of nHAp as well as the signals at 964, 566, 603, and 635 cm^{-1} should be attributed to the phosphate groups (Hakimimehr, Liu, & Troczynski, 2005; Nair, Suresh Babu, Varma, & John, 2008). The relative peaks for nano-HAp can also be observed in the spectra of chitin/nano-HAp hydrogels, confirming the presence of hydroxyapatite nanoparticles in the chitin hydrogel networks. As mentioned in Section 2, nano-HAp content of Gel2 was higher than that of Gel1. Therefore, the intensity of the peaks for phosphate groups increased with the increasing of nano-HAp content of the samples.

The thermal stability of nano-hydroxyapatite, chitin hydrogel, and chitin/nHAp hydrogels was determined by themogravimetric analysis (TGA). As shown in Fig. 2, the mass of nano-HAp changed slightly during the heating process from 40 to 800 °C. The weight of the chitin hydrogel decreased sharply from 250 to 550 °C, and decomposed completely at about 700 °C. For hybrid hydrogels, the weight loss below 100 °C was attributed to the release of moisture from samples. Subsequently, two steps of active weight loss can be observed with elevating temperature. The first step in the temperature range of 200–350 °C was assigned to the decomposition of glycosidic bonds in the hydrogel networks. The second step at 350–650 °C was due to the further decomposition of hydrogel networks into small molecules. In the temperature range from 700 °C to 800 °C, no decrement could be found in the curves, indicating that the hydrogel networks were completely decomposed. At 800 °C, the remnant content of Gel1 was about 6%, whereas that of Gel2 was 16%, due to the presence of nHAp. The swelling ratio of Gel1 and Gel2 was about 88 and 82 g/g, respectively. So the water contents in the hydrogels were 98.9% for Gel1 and 98.8% for Gel2.

The crystalline structures of nano-hyroxyapatite and chitin/nHAp hydrogels were investigated with WAXD and are shown in Fig. 3. The diffraction peaks at 2θ = 25.8, 28, 29, 31.8, 32.9, 34.1, 40, 46.8, 48.1, 49.6, 50.5, 52.1, and 53° were assigned to (0 0 2), (1 0 2), (2 1 0), (2 1 1), (3 0 0), (2 0 2), (3 1 0), (2 2 2), (3 1 2), (2 1 3), (3 2 1), (4 1 0), and (4 0 2) of nHAp, respectively (Watanabe & Akashi, 2006). The main peaks of chitin at 2θ = 9.3 and 19.3° were also included in the hybrid hydrogels, corresponding to (0 2 0) and (1 1 0) of chitin. Although the intensity of nHAp crystal decreased in the hydrogels, the position of nHAp crystal changed hardly. These results indicated that the crystalline structure of nHAp was well retained in the chitin hydrogel networks (Li et al., 2010). This result further supported the conclusion of Figs. 1 and 2, that is, nHAP/chitin hybrid nano-material was successfully fabricated in this work.

3.2. Morphology of nHAp and chitin/nHAp hydrogels

From the result of TEM observation, the hydroxyapatite nanoparticles were spherical in shape with a diameter of 10–30 nm

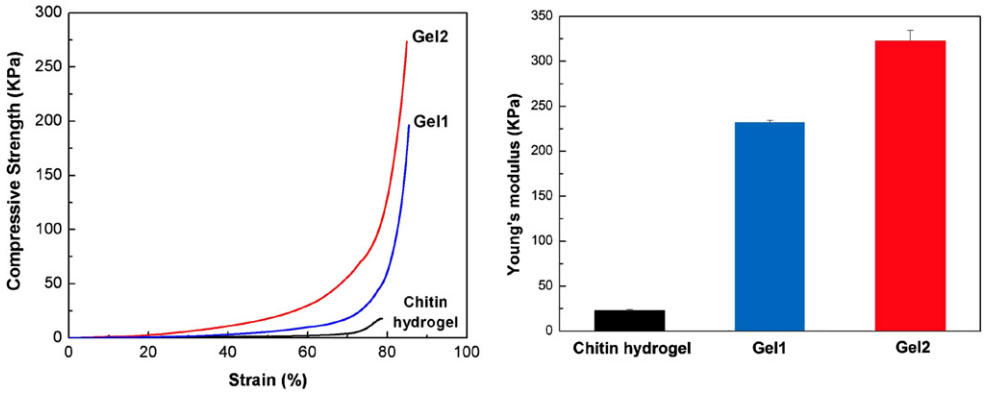

Fig. 6. Compressive stress–strain curves (left) and Young's modulus (right) of chitin hydrogel, Gel1 and Gel2.

(Fig. 4a). At higher magnification, the crystal planes and crystal zone were clearly observed as shown in Fig. 4c. The distribution of nano-particles in the networks of chitin/nano-HAp hybrid hydrogels is very important, which will determine the properties of materials. The TEM images of hydrogel ultrathin section (Fig. 4b) showed that HAp nanoparticles were uniformly dispersed in the hybrid hydrogels, and the crystal structure of nHAp could also be observed at higher magnification (Fig. 4d). According to our previous work, chitin hydrogels had porous structure which is an important factor in the consideration of tissue engineering applications to facilitate cell adhesion, permeability, and spreading (Chang et al., 2011). Therefore, it is necessary to determine the change of porous structure of chitin hydrogels after combining with nano-HAp.

Fig. 5 shows the SEM images of Gel2. The surface of the hydrogels exhibited macroporous structure (a), whereas the cross-section of the hydrogels had interconnecting porous morphology (b) as a result of the phase separation during the freeze-drying process. The distribution of nHAp in the hydrogels can also be observed in the SEM image (c). nHAp dispersed well in the macropore wall of hydrogels without aggregation, indicating a strong interaction between nHAP and chitin. The energy dispersive spectrum (EDS) from SEM (Fig. 5d) indicated that there were C, O, P, and Ca elements in the hybrid hydrogels, which further proved the presence of nHAp in chitin hydrogels. The weight ratio of Ca and P was 29.26% and 14.09%, respectively (see insert of Fig. 5d). Thus the Ca/P weight ratio was 2.08, which approached the value (2.15) calculated from the molecular formula of HAp ($Ca_{10}(PO_4)_6(OH)_2$).

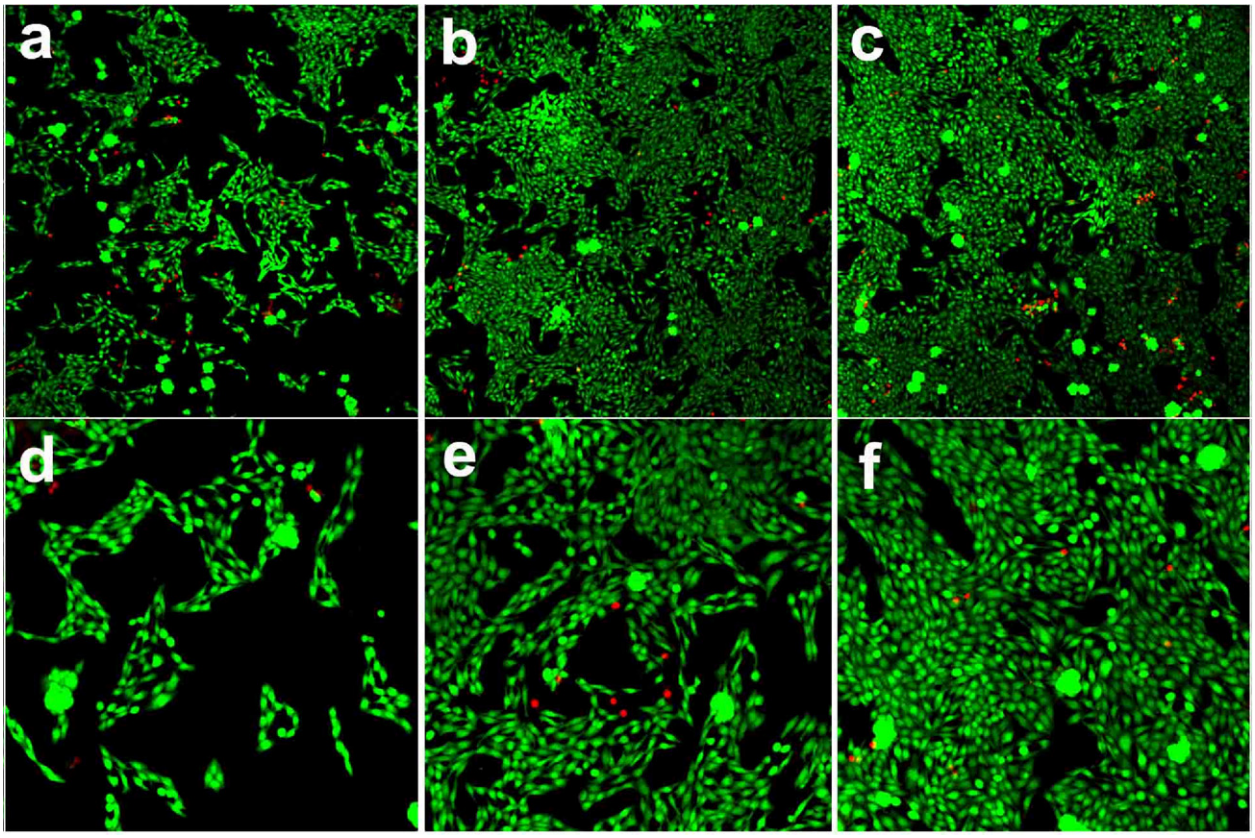

Fig. 7. Confocal microscopy images of live (green) and dead (red) COS-7 cells after 1 day culture on the surface of hydrogel samples: chitin hydrogel (a and d), Gel1 (b and e), and Gel2 (c and f). (For interpretation of the references to color in this figure legend, the reader is referred to the web version of the article.)

3.3. Mechanical properties and biocompatibility of chitin/nano-HAp hydrogels

The compressive stress–strain curves and Young's modulus of chitin hydrogel and chitin/nano-HAp hydrogels are shown in Fig. 6. The compressive strength of all samples increased slowly with the increasing of strain, indicating that hydrogels had good flexibility and toughness. When the strain of hydrogel reached 80%, the compressive strength of hydrogels increased rapidly with a minor change in strain. From the results, the hybrid hydrogels (Gel1 and Gel2) had much higher compressive strength than that of chitin hydrogel. It was noted that Gel2 exhibited about 10 times higher mechanical properties (compressive strength: 274 kPa) than that of the chitin hydrogel. The Young's modulus of chitin hydrogel was 22.8 kPa, whereas the value of Gel2 increased to be 322.4 kPa. These results indicated that the mechanical properties of hydrogels were enhanced significantly by introducing nano-HAp into chitin hydrogel networks. The mechanical property of hydrogel is an important factor for tissue engineering scaffold, because hydrogel must create and maintain a space for tissue development (Eosoly et al., 2010; Tan et al., 2010). On the other hand, the strain of the hybrid hydrogels was similar to that of chitin hydrogel. It revealed that chitin macromolecules played an important role in the improvement of the flexibility of hydrogels, as a result of the formation of the network structure constituted from chitin. The homogeneous macropores in the hydrogel contained stiff chitin chains which supported the macropore wall as shown in Fig. 5c. Moreover, the incorporation of hydroxyapatite nanoparticles into the chitin networks increased obviously the mechanical properties of hydrogels.

COS-7 is a type of COS cell line derived from African green monkey kidney tissue. Herein, COS-7 cells were chosen as model cells to evaluate the biocompatibility of chitin/nano-HAp hydrogels through seeding cells on the surface of hydrogels. It is difficult to observe growth of cells on hydrogels because of the opaque nature of hybrid hydrogels. Therefore, staining was employed to examine the viability of cells on the surface of hydrogels. Healthy cells had green nuclei, uniform chromatin, and intact cell membranes, while cells in necrosis or in a late stage of apoptosis had red nuclei with damaged cell membranes (Li, Meng, Zhang, Fu, & Lu, 2009). Fig. 7 shows the fluorescence images of COS-7 growth on the hydrogels with staining after culturing for 24 h. In our previous work, chitin hydrogels had good biocompatibility and the 293T cellar viability on hydrogel was more than 90% (Chang et al., 2011). The growth of COS-7 cells on chitin hydrogel was good (Fig. 7a), and spindle-shaped COS-7 cells can be observed clearly at higher magnification. Interestingly, the proliferation of COS-7 cells on the chitin/HAp hydrogels was better than that on chitin hydrogels. These results indicated that the introduction of nano-HAp into chitin hydrogel networks promoted the growth of cells, and improved the biocompatibility of hydrogels. Therefore, the chitin/nHAP hybrid hydrogels have great potential in the biomaterials as scaffolds for bone tissue engineering.

4. Conclusion

Chitin/hydroxyapatite nanocomposite hybrid hydrogels were fabricated successfully by incorporating nHAp into chitin hydrogel networks. The HAp nanoparticles were dispersed homogeneously in the chitin/nHAp hybrid hydrogels formed by cross-linking chitin chains with ECH. The incorporation of the HAP nanoparticles in the chitin gels not only improved the mechanical properties significantly but also enhanced the biocompatibility. These chitin/nHAP hybrid hydrogels exhibited porous structure, high mechanical strength, and excellent biocompatibility. It was possible that these scaffolds provided space and supported for the growth of cell and tissue without damaging adjacent cells in the human body. These results suggested that these hydrogel scaffolds were good candidates for bone tissue engineering.

Acknowledgments

This work was supported by National Basic Research Program of China (973 Program, 2010CB732203), and National Natural Science Foundation of China (20874079). Dr. Chang thanks Grant-in-Aid for Japan Society for the Promotion of Science (JSPS) Postdoctoral Fellowships for Foreign Researchers.

References

Cai, X., Chen, L., Jiang, T., Shen, X., Hu, J., & Tong, H. (2011). Facile synthesis of anisotropic porous chitosan/hydroxyapatite scaffolds for bone tissue engineering. *Journal of Materials Chemistry*, *21*(32), 12015–12025.

Chang, C., Chen, S., & Zhang, L. (2011). Novel hydrogels prepared via direct dissolution of chitin at low temperature: Structure and biocompatibility. *Journal of Materials Chemistry*, 3865–3871.

Eosoly, S., Brabazon, D., Lohfeld, S., & Looney, L. (2010). Selective laser sintering of hydroxyapatite/poly-ε-caprolactone scaffolds. *Acta Biomaterialia*, *6*(7), 2511–2517.

Grande, C. J., Torres, F. G., Gomez, C. M., & Carmen Bañó, M. (2009). Nanocomposites of bacterial cellulose/hydroxyapatite for biomedical applications. *Acta Biomaterialia*, *5*(5), 1605–1615.

Hakimimehr, D., Liu, D. M., & Troczynski, T. (2005). In situ preparation of poly (propylene fumarate)–hydroxyapatite composite. *Biomaterials*, *26*(35), 7297–7303.

He, M., Chang, C., Peng, N., & Zhang, L. (2012). Structure and properties of hydroxyapatite/cellulose nanocomposite films. *Carbohydrate Polymers*, *87*, 2512–2518.

Hoare, T. R., & Kohane, D. S. (2008). Hydrogels in drug delivery: Progress and challenges. *Polymer*, *49*(8), 1993–2007.

Jeong, S. I., Ko, E. K., Yum, J., Jung, C. H., Lee, Y. M., & Shin, H. (2008). Nanofibrous poly (lactic acid)/hydroxyapatite composite scaffolds for guided tissue regeneration. *Macromolecular Bioscience*, *8*(4), 328–338.

Jonker, A., Lowik, D. W., & van Hest, J. C. M. (2012). Peptide and protein-based hydrogels. *Chemistry of Materials*, *24*(5), 759–773.

Kopecek, J. (2009). Hydrogels: From soft contact lenses and implants to self-assembled nanomaterials. *Journal of Polymer Science Part A: Polymer Chemistry*, *47*(22), 5929–5946.

Kumar, P., Srinivasan, S., Lakshmanan, V. K., Tamura, H., Nair, S., & Jayakumar, R. (2011). [beta]-Chitin hydrogel/nano hydroxyapatite composite scaffolds for tissue engineering applications. *Carbohydrate Polymers*, *85*, 584–591.

Lee, K. Y., & Mooney, D. J. (2001). Hydrogels for tissue engineering. *Chemical Reviews*, *101*(7), 1869–1880.

Li, L., Kommareddy, K., Pilz, C., Zhou, C., Fratzl, P., & Manjubala, I. (2010). In vitro bioactivity of bioresorbable porous polymeric scaffolds incorporating hydroxyapatite microspheres. *Acta Biomaterialia*, *6*(7), 2525–2531.

Li, L., Meng, L., Zhang, X., Fu, C., & Lu, Q. (2009). The ionic liquid-associated synthesis of a cellulose/SWCNT complex and its remarkable biocompatibility. *Journal of Materials Chemistry*, *19*(22), 3612–3617.

Nair, M. B., Suresh Babu, S., Varma, H., & John, A. (2008). A triphasic ceramic-coated porous hydroxyapatite for tissue engineering application. *Acta Biomaterialia*, *4*(1), 173–181.

Richter, A., Paschew, G., Klatt, S., Lienig, J., Arndt, K. F., & Adler, H. J. P. (2008). Review on hydrogel-based pH sensors and microsensors. *Sensors*, *8*(1), 561–581.

Rossi, A. L., Barreto, I. C., Maciel, W. Q., Rosa, F. P., Rocha-Leão, M. H., Werckmann, J., et al. (2012). Ultrastructure of regenerated bone mineral surrounding hydroxyapatite–alginate composite and sintered hydroxyapatite. *Bone*, *50*, 301–310.

Ryan, D. M., & Nilsson, B. L. (2011). Self-assembled amino acids and dipeptides as noncovalent hydrogels for tissue engineering. *Polymer Chemistry*, *3*(1), 18–33.

Sun, F., Zhou, H., & Lee, J. (2011). Various preparation methods of highly porous hydroxyapatite/polymer nanoscale biocomposites for bone regeneration. *Acta Biomaterialia*, *7*, 3813–3828.

Swetha, M., Sahithi, K., Moorthi, A., Srinivasan, N., Ramasamy, K., & Selvamurugan, N. (2010). Biocomposites containing natural polymers and hydroxyapatite for bone tissue engineering. *International Journal of Biological Macromolecules*, *47*(1), 1–4.

Tan, R., Feng, Q., She, Z., Wang, M., Jin, H., Li, J., et al. (2010). In vitro and in vivo degradation of an injectable bone repair composite. *Polymer Degradation and Stability*, *95*(9), 1736–1742.

Van Vlierberghe, S., Dubruel, P., & Schacht, E. (2011). Biopolymer-based hydrogels as scaffolds for tissue engineering applications: A review. *Biomacromolecules*, *12*, 1387–1408.

Watanabe, J., & Akashi, M. (2006). Novel biomineralization for hydrogels: Electrophoresis approach accelerates hydroxyapatite formation in hydrogels. *Biomacromolecules*, *7*(11), 3008–3011.

Wei, G., & Ma, P. X. (2004). Structure and properties of nano-hydroxyapatite/polymer composite scaffolds for bone tissue engineering. *Biomaterials*, *25*(19), 4749–4757.

Zhang, L., Tang, P., Xu, M., Zhang, W., Chai, W., & Wang, Y. (2010). Effects of crystalline phase on the biological properties of collagen–hydroxyapatite composites. *Acta Biomaterialia*, *6*(6), 2189–2199.
Zhou, H., & Lee, J. (2011). Nanoscale hydroxyapatite particles for bone tissue engineering. *Acta Biomaterialia*, *7*, 2769–2781.
Zhu, J. (2010). Bioactive modification of poly (ethylene glycol) hydrogels for tissue engineering. *Biomaterials*, *31*(17), 4639–4656.
Zohuriaan-Mehr, M., Omidian, H., Doroudiani, S., & Kabiri, K. (2010). Advances in non-hygienic applications of superabsorbent hydrogel materials. *Journal of Materials Science*, *45*(21), 5711–5735.